ACS APPLIED MATERIALS & INTERFACES

Research Article

www.acsami.org

Room-Temperature Sol–Gel Derived Molybdenum Oxide Thin Films for Efficient and Stable Solution-Processed Organic Light-Emitting Diodes

Qiang Fu,[†,‡] Jiangshan Chen,[*,†] Changsheng Shi,[†] and Dongge Ma[†]

[†]State Key Laboratory of Polymer Physics and Chemistry, Changchun Institute of Applied Chemistry, Chinese Academy of Sciences, Changchun, 130022, P. R. China

[‡]University of Chinese Academy of Sciences, Beijing, 100049, P. R. China

Supporting Information

ABSTRACT: Molybdenum oxide (MoO_3) thin films were prepared by sol–gel methods at room temperature from the precursors of MoO_3 powder mixing into NH_3 or H_2O_2 solution and then directly treated by UV-ozone instead of widely used high-temperature annealing. Atomic force microscopy (AFM), X-ray photoelectron spectroscopy (XPS), and ultraviolet photoelectron spectroscopy (UPS) characteristics demonstrated that the room-temperature sol–gel derived MoO_3 thin films exhibited excellent uniformity, unchanged chemical structure, and high work function. For the first time, the novel solution-processed MoO_3 thin films were successfully applied as the hole injection layers (HILs) for solution-processed organic light-emitting diodes (OLEDs). The efficiencies of the resulting OLEDs were comparable or even higher than that of the device using PEDOT:PSS as the HIL. More importantly, the lifetimes of the solution-processed OLEDs are improved by nearly 2 orders of magnitude. This study should provide a potential approach to develop low-cost, high-performance, and long-lifetime OLEDs for practical applications.

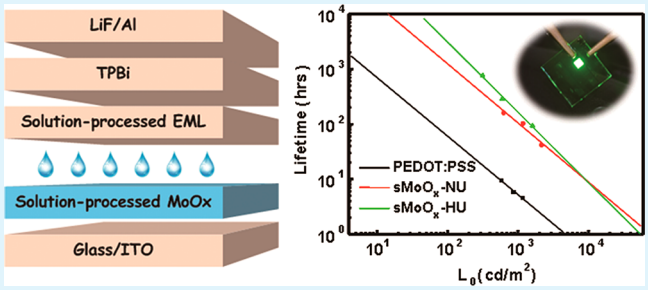

KEYWORDS: *molybdenum oxide, hole injection, solution process, interface stability, organic light-emitting diodes*

INTRODUCTION

Organic light-emitting diodes (OLEDs) have drawn much attention during the past decades due to their potential applications in flat-panel displays and solid-state lighting.[1−3] Currently, great efforts have been made to develop small molecule OLEDs by solution process, which is expected to realize a trade-off between low cost and high performance.[4−7] Although recent advances in efficiencies of the solution-processed OLEDs have been achieved, there is still a big challenge to improve the lifetime to meet the requirement of practical applications.[8,9] At the mention of the stability of solution-processed OLEDs, we have to take account of the issue at the interface between the indium tin oxide (ITO) anode and the hole injection layer (HIL), which is considered as one of the main reasons to accelerate degradation.[10] The common HIL material of poly(ethylenedioxythiophene):poly-(styrene sulfonate) (PEDOT:PSS) has been exclusively used in the solution-processed OLEDs due in part to its broad applicability, reproduction, and availability. However, the evidence has suggested that PEDOT:PSS plays a disadvantageous role in OLED degradation because of its acidic nature (typical pH value of 1.58), which etches the ITO and accelerates the diffusion of indium into the organic layer.[10,11] In addition, PEDOT:PSS is hygroscopic, and its conductivity and work function can be varied with moisture and oxygen.[12,13] Therefore, it is imperative to develop other promising candidates to replace PEDOT:PSS for solution-processed OLEDs.

Vacuum-evaporation-deposited transition metal-oxides (TMOs), such as molybdenum-oxide (MoO_3), vanadium-oxide (V_2O_5), and tungsten-oxide (WO_3), have been widely used as HILs for OLEDs to improve device efficiency and stability due to their suitable electronic properties, intrinsic stability, and high work function.[14−16] Recently, solution-processed TMO films have been successfully prepared to be used as the hole extraction layers in organic solar cells.[17−25] However, the report on the utilization of TMOs as solution-processed HILs in OLEDs is still scarce.

In this paper, we prepared MoO_x thin films by sol–gel methods from the precursor solutions by mixing MoO_3 powder into ammonia (NH_3) or hydrogen peroxide (H_2O_2) water and then treating by UV-ozone without pre- and postannealing. The solution-processed MoO_x ($sMoO_x$) films exhibited excellent uniformity and good hole-injection property after the UV-ozone treatment and were successfully applied as the HILs for solution-processed phosphorescent OLEDs. The efficiencies of

Received: February 26, 2013
Accepted: May 21, 2013
Published: May 21, 2013

   dx.doi.org/10.1021/am4007319 | ACS Appl. Mater. Interfaces 2013, 5, 6024–6029

the fabricated OLEDs with the $sMoO_x$ HILs were found to be comparable to or even higher than that of the PEDOT:PSS-based device. More encouragingly, the lifetime of the solution-processed phosphorescent OLEDs was significantly improved by the replacement of PEDOT:PSS with the $sMoO_x$.

EXPERIMENTAL SECTION

Preparation of MoO_3 Precursor Solution. The precursor solutions were prepared by mixing MoO_3 powder (99.999%, Sigma-Aldrich) into excess NH_3 (25%, J&K Scientific Ltd.) or H_2O_2 (30%, Sigma-Aldrich) with reflux (0.5 h at 60 °C in air). The clear solutions (colorless for NH_3 solution and yellow for H_2O_2 solution) were then cooled to room temperature and rested over several days. The viscosity and concentration of the solution were further adjusted by adding polyethylene glycol (average M_n 200, Sigma-Aldrich) and 2-ethoxyethanol (Sigma-Aldrich).

Formation of Thin Films and Characterization. The obtained precursor solutions were spin-coated on ITO substrates with a sheet resistance of 10 Ω/square. The ITO substrates were ultrasonically cleaned with detergent, deionized water, acetone, and isopropanol and then dried by blowing nitrogen. The solution-processed films were then treated with UV radiation from a low-pressure mercury lamp (SEN Lights PL16-110) for 30 min. For comparison, the films were also treated by annealing at the temperature of 280 °C for 30 min on a hot plate in the nitrogen-protected glovebox. The surface morphologies of the films were measured by atomic force microscopy (AFM) (SPA 300HV with a SPI 3800N Probe Station, Seiko Instruments Inc., Japan) in tapping mode. The electronic characteristics of the films were performed by X-ray photoelectron spectroscopy (XPS) with an Al Kα X-ray source (1486.6 eV) and ultraviolet photoelectron spectroscopy (UPS) with a He discharge lamp (UV light of 21.22 eV) (Thermo Electron Corporation, ESCALAB 250). The resolution of the spectra was 0.3 eV for XPS and 0.1 eV for UPS. The UPS measurements were performed with a −8 V bias applied to the samples to enable the measurement of the secondary electrons cutoff. Grazing-angle XRD spectra measurements were carried out in an out-of plane, grazing incidence geometry on a Rigaku SmartLab diffraction system with a Cu Kα source. The integration time was 10 min/degree, and the incident beam was fixed at 0.2°.

Device Fabrication and Measurements. The solution-processed metal oxide films and PEDOT:PSS were used as the HILs formed on ITO. The emission layers (EMLs) of $Ir(ppy)_3$ doped into TCTA were then spin-coated on top of the HILs from chlorobenzene and baked at 120 °C in a vacuum oven for 30 min to remove residual solvent. Following that, the samples were transferred to a thermal evaporator chamber (pressure less than 5×10^{-4} Pa) for the sequent deposition of TPBi, LiF, and Al by thermal evaporation. The overlap between ITO and Al electrodes was 16 mm^2 as the active emissive area of the devices. The current−brightness−voltage characteristics were tested by a Keithley source measurement unit (Keithley 2400 and Keithley 2000) with a calibrated silicon photodiode. The lifetime measurements were carried out at a fixed current density in a glovebox.

RESULTS AND DISSCUSION

Surface Characteristics of $sMoO_x$ Thin Films. The surface characteristics of the $sMoO_x$ films were first examined by atomic force microscopy (AFM). Figure 1 shows the AFM images of the $sMoO_x$ films spin-coated on ITO substrates with and without UV-ozone treatment. It can be seen that obvious aggregation and clusters appear in the pristine films from NH_3 solution ($sMoO_x$-NP) and H_2O_2 solution ($sMoO_x$-HP), and the variations of peak to valley are over 10 nm. The root-mean-square (RMS) surface roughness of $sMoO_x$-NP and $sMoO_x$-HP are 2.247 and 4.716 nm, respectively. However, the UV-ozone-treated $sMoO_x$ films of $sMoO_x$-NU (from NH_3) and $sMoO_x$-HU (from H_2O_2) become much more smooth and uniform, and their RMS surface roughness decreases to 0.571 and 1.573

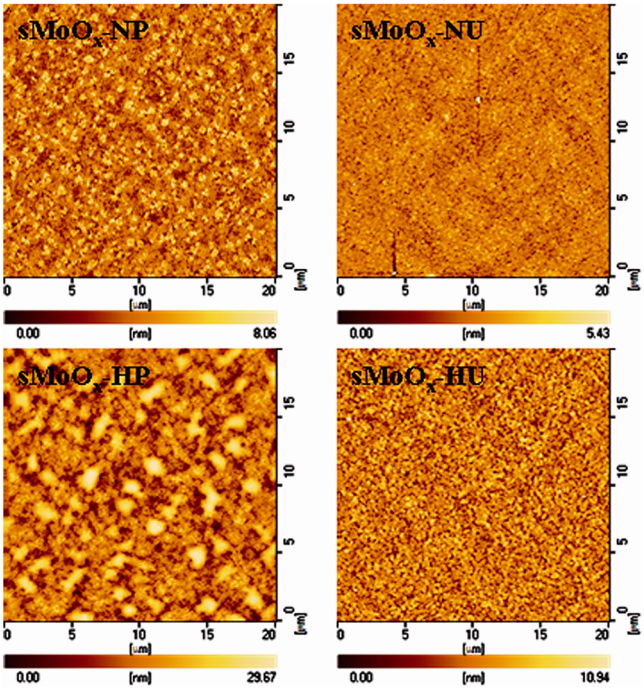

Figure 1. AFM images of the $sMoO_x$ films formed on ITO substrates before and after UV-ozone treatment.

nm, respectively, which are even less than those of the bare ITO (2.622 nm) and the vacuum-evaporation-deposited MoO_3 ($eMoO_x$-AE) film (2.865 nm) (see Supporting Information (SI) S1). To date, it was reported that the annealing treatment is the necessary process to convert the MoO_3 precursors to the dry films by hydrolysis, which can provide the sufficient morphological and electronic properties to be conducive to organic solar cells.[17,20−24] Here, we also prepared the $sMoO_x$ films (denoted as $sMoO_x$-NA and $sMoO_x$-HA from NH_3 and H_2O_2, respectively) by annealing at 280 °C in a nitrogen-protected glovebox. It was found that the annealed films are also defect-free and uniform but are still rougher than the UV-ozone treated films (see Supporting Information S1). Although the detailed mechanism of the conversion of the precursors to the novel dense $sMoO_x$ films by UV-ozone treatment is not clear, the photolysis effect ought to play a key role. The organic additives of polyethylene glycol and 2-ethoxyethanol could be degraded to CO_2 and H_2O by UV-ozone irradiation. The decomposition of polyethylene glycol in electroplating solution by UV-ozone was reported before.[26] To clarify the degradation of the organic additives in the $sMoO_x$ films by UV-ozone treatment, X-ray photoelectron spectroscopy (XPS) measurements were carried out, and the spectra of C 1s and O 1s in the $sMoO_x$ films before and after UV-ozone treatment are shown in Figure 2. The pristine films exhibit a strong C 1s peak at 287.2 eV, which corresponds to C−O−C(H) from the organic additives. After UV-ozone treatment, the peak at 287.2 eV disappears. Additionally, the pristine films exhibit an extra O 1s peak at 533.5 eV, which also corresponds to C−O−C(H). After UV-ozone treatment, the extra peak at 533.5 eV disappears, and only the peak at 530.9 eV remains, which should correspond to the bond between O and Mo. The changes of XPS spectra of C 1s and O 1s clearly demonstrate that polyethylene glycol and 2-ethoxyethanol are removed by UV-ozone, inferring that the photolysis should occur during the conversion of precursors to dense $sMoO_x$ films.

dx.doi.org/10.1021/am4007319 | ACS Appl. Mater. Interfaces 2013, 5, 6024−6029

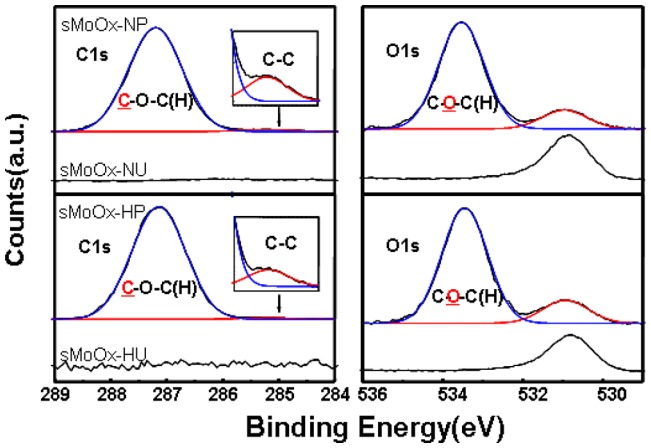

Figure 2. XPS spectra (C 1s and O 1s core level peaks) of the $sMoO_x$ films before and after UV-ozone treatment.

In addition, X-ray diffraction (XRD) measurements shown in Supporting Information S2 were performed to characterize the solution-processed metal-oxide films, and no discernible diffraction peaks were found in the XRD spectra, indicating the amorphous or nanocrystalline nature of these films.

Electronic Properties of $sMoO_x$ Thin Films. XPS measurements were carried out to further investigate the surface characteristics of the solution-processed films treated by UV-ozone and annealing. Figure 3 shows the Mo 3d core level

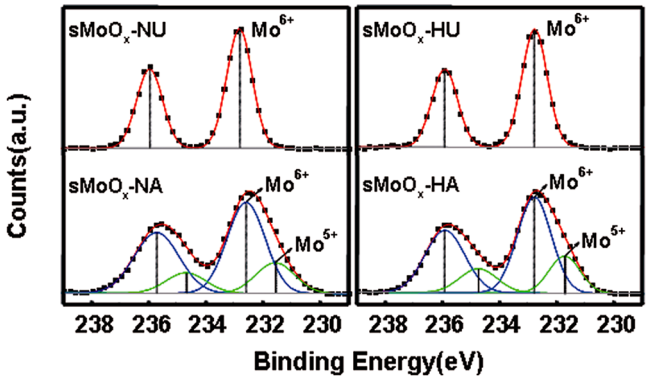

Figure 3. XPS spectra (Mo 3d core level peaks) of the $sMoO_x$ films treated by UV-ozone and annealing.

peaks of $sMoO_x$-NU, $sMoO_x$-HU, $sMoO_x$-NA, and $sMoO_x$-HA. In the UV-ozone-treated $sMoO_x$ films, the Mo 3d 5/2 peak at 232.7 eV and the Mo 3d 3/2 peak at 235.9 eV are symmetric without a shoulder, showing that the Mo atoms are mainly in the Mo^{6+} oxidation state.[17,20] This clearly indicates that a nearly stoichiometric MoO_3 exists in the UV-ozone films. However, the binding energy peaks of the annealed films broaden obviously, corresponding to the formation of the Mo^{5+} species.[17,20−22] The Mo^{5+} state was also found in the air exposed $eMoO_x$-AE film (see Supporting Information S3), which is consistent with the reported study.[27] The ratio between Mo^{5+} and Mo^{6+} in the metal oxide films was calculated by fitting the XPS spectra of the Mo 3d core level, thus the Mo:O stoichiometry can be determined (see Supporting Information S4).[17] The XPS analysis demonstrated that the UV-ozone treatment is preferred to annealing to maintain the chemical and electronic characteristics of $sMoO_x$. Moreover, it should be noted that the UV-ozone is advantageous over high-temperature annealing for the fabrication of organic electronic devices on flexible plastic substrates.

For the application of the UV-ozone treated $sMoO_x$ as HILs in OLEDs, it is vital to ascertain their work functions (WFs) to evaluate their hole-injection capability. For this purpose, we investigated the electronic structures of the $sMoO_x$ films on ITO substrates using ultraviolet photoelectron spectroscopy (UPS). Figure 4 shows the UPS spectra of the $sMoO_x$-NU and

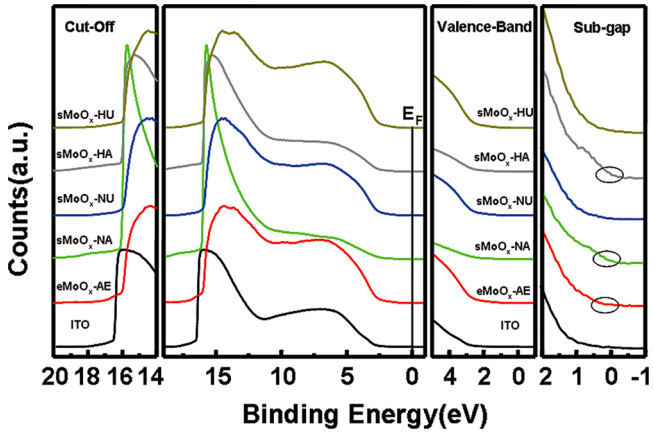

Figure 4. UPS spectra of the $sMoO_x$ films on ITO treated by UV-ozone and annealing. The spectra of ITO and air-exposed $eMoO_x$-AE are shown for comparison. The secondary-electron cutoff (left), valence-band region (right), and magnified subgap region (far right) are included.

$sMoO_x$-HU, and the ones of ITO, $sMoO_x$-NA, $sMoO_x$-HA, and $eMoO_x$-EA are given for comparison. Magnified regions of the photoemission cutoff, valence band, and subgap states are included. The photoemission onsets of $sMoO_x$-NU and $sMoO_x$-HU were found at 15.9 eV, thus the corresponding WF was determined to be 5.3 eV, which is 0.6 eV higher than that of ITO (4.7 eV). Similarly, the WF values of $sMoO_x$-NA and $sMoO_x$-HA were determined to be 5.1 eV. This suggests that the UV-ozone treated metal oxides are more suitable to replace PEDOT:PSS as the HILs for the solution-processed OLEDs compared to the annealed counterparts. At the same time, the ionization energies (IEs) can be derived from the valence band edges, and the IEs of $sMoO_x$-NU and $sMoO_x$-HU were found to be 8.1 and 8.0 eV, respectively. The obtained WF and IE of $sMoO_x$-NU and $sMoO_x$-HU are very similar to those of $eMoO_x$-EA. It should be pointed out that the subgap states at the binding energies of 0.2−0.4 eV were found in the films of $sMoO_x$-NA, $sMoO_x$-HA, and $eMoO_x$-AE, which further proved the existence of Mo^{5+} species observed by the XPS analysis as discussed above.[17]

Performances of Solution-Processed OLEDs with $sMoO_x$ HILs. Solution-processed small-molecule phosphorescent OLEDs using the UV-ozone treated $sMoO_x$ films as HILs were then examined. The conventional device structure fabricated here is ITO/HILs/TCTA:$Ir(ppy)_3$ (10 wt %, 40 nm)/TPBi (40 nm)/LiF (1 nm)/Al (100 nm), and the chemical structures of the used organic materials are shown in Figure 5. The emission layer (EML) of TCTA:$Ir(ppy)_3$ was spin-coated on top of the solution-processed HILs, and TPBi, LiF, and Al were subsequently deposited by vacuum evaporation to function as the electron transport layer, electron injection layer, and cathode, respectively. We change the concentration of MoO_3 by varying the amount of polyethylene

dx.doi.org/10.1021/am4007319 | ACS Appl. Mater. Interfaces 2013, 5, 6024−6029

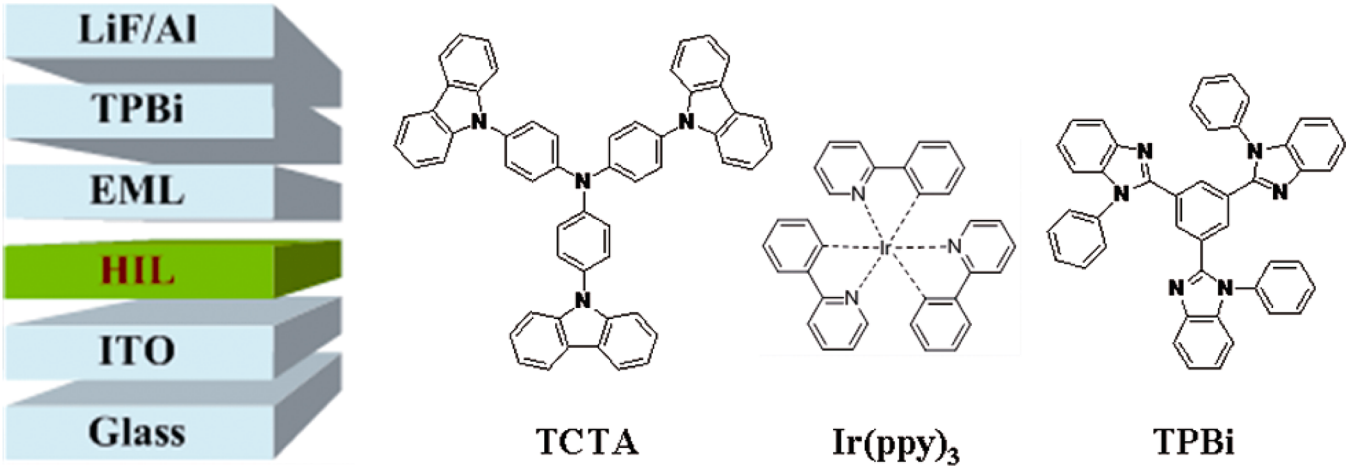

Figure 5. Device configuration of the simple green OLEDs and molecular structures of the used organic materials.

Table 1. Summary of Device Performance in the Solution-Processed OLEDs

HIL	V_{on} [a] (V)	CE_{max} [b] (cd/A)	PE_{max} [b] (lm/W)	CE_{100} [c] (cd/A)	PE_{100} [c] (lm/W)	CE_{1000} [d] (cd/A)	PE_{1000} [d] (lm/W)
PEDOT:PSS	3.0	55.8	54.7	51.2	39.6	46.6	28.1
$sMoO_x$-NU	3.1	58.6	53.7	56.2	39.3	48.5	25.4
$sMoO_x$-HU	3.0	53.7	54.7	51.0	36.8	46.4	24.8
$sMoO_x$-NA	3.1	33.9	32.6	32.6	23.8	27.1	15.8
$sMoO_x$-HA	3.0	38.9	35.5	38.5	31.4	33.2	21.2

[a]The voltage at 1 cd/m^2. [b]Maximum current efficiency (CE) and power efficiency (PE). [c]The efficiencies at 100 cd/m^2. [d]The efficiencies at 1000 cd/m^2.

glycol and 2-ethoxyethanol to obtain different film thickness. Supporting Information S5 depicts the performances of the OLEDs based on different concentrations of MoO_3. The optimized device efficiencies are obtained at the concentration of 10 mg/mL, which corresponds to a thickness of about 6 nm. For comparison, the devices with PEDOT:PSS, $sMoO_x$-NA, and $sMoO_x$-HA as the HILs were also fabricated. The performance characteristics were given in Supporting Information S6. The current density of the devices using the annealed $sMoO_x$ as the HILs is higher than those of the devices using the UV-ozone treated $sMoO_x$ as the HILs, but the efficiency of the devices with annealed $sMoO_x$ is lower than the devices with UV-ozone treated $sMoO_x$. The device performances and the detailed parameters are summarized in Table 1. The devices using the $sMoO_3$-NU and $sMoO_3$-HU films as the HILs show the maximum efficiencies of 58.6 cd A^{-1} (53.7 lm W^{-1}) and 53.7 cd A^{-1} (54.7 lm W^{-1}), respectively, which are comparable to that using PEDOT:PSS. Even at the high brightness of 1000 cd m^{-2}, the current efficiencies still reach 48.5 and 46.4 cd A^{-1} for the OLEDs based on the $sMoO_x$-NU and $sMoO_x$-HU HILs, respectively. The higher efficiency in the solution-processed OLEDs based on the $sMoO_x$ treated by UV-ozone could be mainly attributed to the higher charge balance in the devices. In addition, the character of the solution-processed EML should also influence the performance of the resulting devices. Thus, the surface morphologies of the EML on different HILs were characterized by AFM. The AFM images are given in Supporting Information S7. It was found that the EMLs on $sMoO_x$-NU and $sMoO_x$-HU are slightly rougher than that on PEDOT:PSS but are smoother than that on the annealed metal oxides.

It was demonstrated that the stability of OLEDs fabricated by vacuum evaporation was significantly improved by evaporated MoO_x.[16,28] However, until now, research results about solution-processed OLEDs are limited. We expect our obtained $sMoO_x$ to be used to improve the stability of the solution-processed OLEDs. Thus, the lifetime measurements were carried out in a glovebox at a constant driving current density. Figure 6a shows the characteristics of brightness−time ($L-T$) at different initial brightness values (L_0) for the devices with PEDOT:PSS, $sMoO_x$-NU, and $sMoO_x$-HU as the HILs. Figure 6b gives the relationship between lifetime and brightness according to the equation of $L_0^n \times T_{1/2}$ = constant, where $T_{1/2}$ is the time needed for the brightness to decrease to 50% of the initial value and n is an acceleration factor.[29,30] It is clearly seen that the solution-processed OLEDs using UV-ozone treated $sMoO_x$ possess significantly improved stability compared to that using PEDOT:PSS. The lifetimes of the simple devices with $sMoO_x$ thin films as the HILs are near 2 orders of magnitude higher than that of the PEDOT:PSS-based OLED. This result will encourage us to further optimize the device structure and processing technology to develop more stable solution-processed OLEDs based on the solution-processed metal oxides.

CONCLUSIONS

In summary, we demonstrated a novel method to prepare MoO_x thin films by solution processes associated with UV-ozone treatment and successfully utilized them as the HILs to achieve efficient and stable solution-processed OLEDs. The obtained amorphous $sMoO_x$ films give excellent morphologies, which is benefiting for subsequently solution-processing the EMLs. The XPS and UPS analysis demonstrated that the UV-ozone treated $sMoO_x$ films possess sufficient electronic properties to function as the HILs to replace PEDOT:PSS. We also found that the UV-ozone treatment is preferred

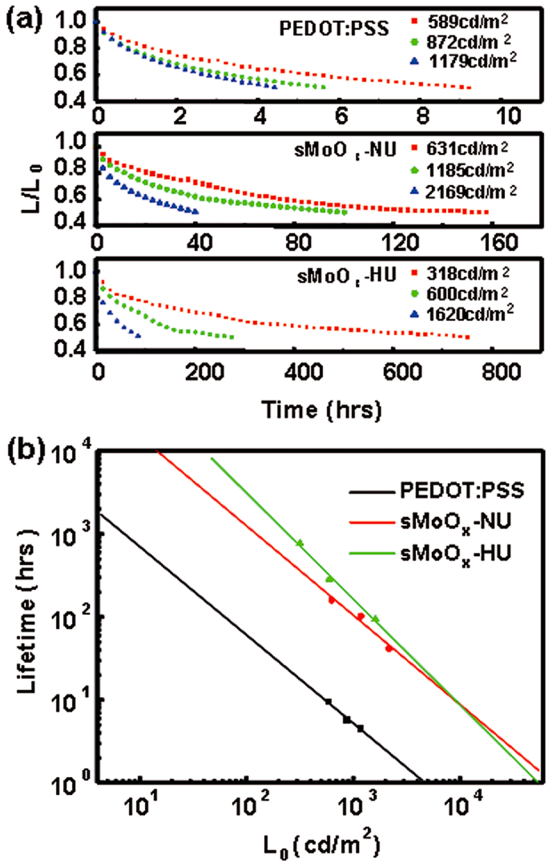

Figure 6. Characteristics of brightness−time at different initial brightness (a) and relationship between brightness and half-life (b) in the solution-prcoessed OLEDs based on PEDOT:PSS, $sMoO_x$-NU, and $sMoO_x$-HU. The half-lives are estimated with a fitted acceleration coefficient of n = 1.06, 1.08, and 1.28, respectively.

compared to the widely used annealing method to retain the chemical and electronic characteristics of the metal oxides during the solution process. This study should provide a potential approach to develop low-cost, high-efficiency, and long-lifetime OLEDs for practical applications.

■ ASSOCIATED CONTENT

Ⓢ Supporting Information

Further details about AFM images, XPS data, Mo:O stoichiometry of metal oxide films, and AFM images of emission layers based on different hole injection layers and the detailed experimental procedures. This material is available free of charge via the Internet at http://pubs.acs.org.

■ AUTHOR INFORMATION

Corresponding Author

*Tel.: +86 431 85262807. Fax: +86 431 85262873. E-mail: jschen@ciac.jl.cn.

Author Contributions

The manuscript was written through contributions of all authors. All authors have given approval to the final version of the manuscript.

Notes

The authors declare no competing financial interest.

■ ACKNOWLEDGMENTS

This work was supported by the National Basic Research Program of China (973 program No. 2013CB834805, 2009CB623604), National Natural Science Foundation of China (21161160442, 61036007), the Science Fund for Creative Research Groups of NSFC (20921061), and the Foundation of Jilin Research Council (201105028, 2012ZDGG001).

■ REFERENCES

(1) Tang, C. W.; Vanslyke, S. A. *Appl. Phys. Lett.* **1987**, *51*, 913−915.
(2) Burroughes, J. H.; Bradely, D. D. C.; Brown, A. R.; Marks, R. N.; Mackay, K.; Friend, R. H.; Burn, P. L.; Holmes, A. B. *Nature* **1990**, *347*, 539−541.
(3) Reineke, S.; Lindner, F.; Schwartz, G.; Seidler, N.; Walzer, K.; Lussem, B.; Leo, K. *Nature* **2009**, *459*, 234−U116.
(4) Wu, H. B.; Zhou, G. J.; Zou, J. H.; Ho, C. L.; Wong, W. Y.; Yang, W.; Peng, J. B.; Cao, Y. *Adv. Mater.* **2009**, *21*, 4181−4184.
(5) Yook, K. S.; Jang, S. E.; Jeon, S. O.; Lee, J. Y. *Adv. Mater.* **2010**, *22*, 4479−4483.
(6) Gong, S. L.; Fu, Q.; Wang, Q.; Yang, C. L.; Zhong, C.; Qin, J. G.; Ma, D. G. *Adv. Mater.* **2011**, *23*, 4956−4959.
(7) Huang, H.; Fu, Q.; Zhuang, S. Q.; Liu, Y. K.; Wang, L.; Chen, J. S.; Ma, D. G.; Yang, C. L. *J. Phys. Chem. C* **2011**, *115*, 4872−4878.
(8) So, F.; Kondakov, D. *Adv. Mater.* **2010**, *22*, 3762−3777.
(9) Jørgensen, M.; Norrman, K.; Gevorgyan, S. A.; Tromholt, T.; Andreasen, B.; Krebs, F. C. *Adv. Mater.* **2012**, *24*, 580−612.
(10) de Jong, M. P.; van IJzendoorn, L. J.; de Voigt, M. J. A. *Appl. Phys. Lett.* **2000**, *77*, 2255−2257.
(11) Duan, L.; Hou, L. D.; Lee, T.-W.; Qiao, J.; Zhang, D. Q.; Dong, G. F.; Wang, L. D.; Qiu, Y. *J. Mater. Chem.* **2010**, *20*, 6392−6407.
(12) Nardes, A. M.; Kemerink, M.; de Kok, M. M.; Vinken, E.; Maturova, K.; Janssen, R. A. J. *Org. Electron.* **2008**, *9*, 727−734.
(13) Huang, J. S.; Miller, P. F.; Wilson, J. S.; de Mello, A. J.; de Mello, J. C.; Bradley, D. D. C. *Adv. Funct. Mater.* **2005**, *15*, 290−296.
(14) Meyer, J.; Hamwi, S.; Kröger, M.; Kowalsky, W.; Riedl, T.; Kahn, A. *Adv. Mater.* **2012**, *24*, 5408−5427.
(15) Meyer, J.; Winkler, T.; Hamwi, S.; Schmale, S.; Johannes, H.-H.; Weimann, T.; Hinze, P.; Kowlasky, W.; Riedl, T. *Adv. Mater.* **2008**, *20*, 3839−3843.
(16) You, H.; Dai, Y.; Zhang, Z.; Ma, D. *J. Appl. Phys.* **2007**, *101*, 026105.
(17) Jasieniak, J. J.; Seifter, J.; Jo, J.; Mates, T.; Heeger, A. J. *Adv. Funct. Mater.* **2012**, *22*, 2594−2605.
(18) Choi, H.; Kim, B. S.; Ko, M. J.; Lee, D.-K.; Kim, H.; Kim, S. H.; Kim, K. *Org. Electron.* **2012**, *13*, 959−968.
(19) Zilberberg, K.; Trost, S.; Schmidt, H.; Riedl, T. *Adv. Energy Mater.* **2011**, *1*, 377−381.
(20) Zilberberg, K.; Gharbi, H.; Behrendt, A.; Trost, S.; Riedl, T. *ACS Appl. Mater. Interfaces* **2012**, *4*, 1164−1168.
(21) Girotto, C.; Voroshazi, E.; Cheyns, D.; Heremans, P.; Rand, B. P. *ACS Appl. Mater. Interfaces* **2011**, *3*, 3244−3247.
(22) Hammond, S. R.; Meyer, J.; Widjonarko, N. E.; Ndione, P. F.; Sigdel, A. K.; Garcia, A.; Miedaner, A.; Lloyd, M. T.; Kahn, A.; Ginley, D. S.; Berry, J. J.; Olson, D. C. *J. Mater. Chem.* **2012**, *22*, 3249−3254.
(23) Yang, T. B.; Wang, M.; Cao, Y.; Huang, F.; Huang, L.; Peng, J. B.; Gong, X.; Cheng, S. Z. D.; Cao, Y. *Adv. Energy Mater.* **2012**, *2*, 523−527.
(24) Murase, S.; Yang, Y. *Adv. Mater.* **2012**, *24*, 2459−2462.
(25) Meyer, J.; Khalandovsky, R.; Görrn, P.; Kahn, A. *Adv. Mater.* **2011**, *23*, 70−73.
(26) Chang, C. Y.; Chen, Y. H.; Li, H.; Chiu, C. Y.; Yu, Y. H.; Chiang, P. C.; Ku, Y.; Chen, J. N. *J. Environ. Eng.* **2001**, *127* (10), 908−915.
(27) Zhong, J. Q.; Mao, H. Y.; Wanga, R.; Lin, J. D.; Zhao, Y. B.; Zhang, J. L.; Ma, D. G.; Chen, W. *Org. Electron.* **2012**, *13*, 2793−2800.
(28) Zhao, Y. B.; Chen, J. S.; Chen, W.; Ma, D. G. *J. Appl. Phys.* **2012**, *111*, 043716.

(29) Chu, T.-Y.; Chen, J.-F.; Chen, S.-Y.; Chen, C.-J.; Chen, C. H. *Appl. Phys. Lett.* **2006**, *89*, 053503.
(30) Féry, C.; Racine, B.; Vaufrey, D.; Doyeux, H.; Cinà, S. *Appl. Phys. Lett.* **2005**, *87*, 213502.